Journal of Sustainable Development of Energy, Water and Environment Systems

http://www.sdewes.org/jsdewes

Year 2027, Volume 15, Issue 1, 1140758

Original Research Article

Experimental Study on Optimal Performance of a Film Humidifier for a Small-Scale Thermal Desalination System

Volodymyr Sereda, Yang Liu, Tetiana Podstievaia, Igor Telychko*
National Technical University of Ukraine "Igor Sikorsky Kyiv Polytechnic Institute"
Polytechnichna 6, 03056 Kyiv, Ukraine
e-mail: sereda.volodymyr@lll.kpi.ua

Cite as: Sereda, V., Liu, Y., Podstievaia, T., Telychko, I., Experimental Study on Optimal Performance of a Film Humidifier for a Small-Scale Thermal Desalination System, J.sustain. dev. energy water environ. syst., 15(1), 1140758, 2027, DOI: https://doi.org/10.13044/j.sdewes.d14.0758

ABSTRACT

The paper investigates the design and performance of humidifiers used in low-grade heat-driven desalination systems. It reviews the advantages and limitations of common humidifier types and presents an experimental study of a film-type humidifier configured as a vertical acrylic tube. Experiments examined hydrodynamics and heat and mass transfer over air mass flow rates of 7.4–35 kg/h, water mass flow rates of 10–80 kg/h, inlet water temperatures of 28–59 °C, air pressure drops of 19–324 Pa, water pressure losses of 22.3 kPa, and heater power inputs of 90–554 W. Optimal operating conditions were identified to maximize system performance and energy efficiency. A thermodynamic model based on heat and mass transfer equations was developed and validated. Compared with other humidifier designs, the film-type humidifier achieved the highest evaporation rate at equivalent operating conditions while maintaining minimal aerodynamic and hydraulic resistance, thereby reducing electricity consumption for air and water circulation without performance losses.

KEYWORDS

Energy efficiency, Humidification-dehumidification, Direct-contact exchanger, Thermal desalination, Heat and mass transfer.

INTRODUCTION

Freshwater scarcity is now one of the most pressing global challenges, threatening socio-economic stability and environmental balance across many regions. With population growth, rapid urbanization, and climate change, the demand for freshwater continues to rise, while natural resources remain limited [1]. According to the UN estimates, over two billion people live in regions experiencing severe water shortages, making desalination a promising technology for ensuring access to clean water [2].

Desalination methods are broadly categorized into thermal and membrane technologies [3]. Currently, membrane technologies dominate the desalination technology market, with 90% of desalination plant construction contracts utilizing membranes since 2010. The widespread adoption of membrane technologies is due to their undeniable advantages: continuous desalination capability, high desalination rates, high water recovery and salt removal efficiency, low energy consumption, minimal pre-treatment requirements, and long operational lifespan [4]. However, membrane systems also have significant drawbacks, including the inability to fully remove pesticides, herbicides, and chlorine due to their smaller molecular size compared

* Corresponding author

to water; potential depletion of natural minerals from water; high water waste in the process; degradation of water quality over time; and the need for high-quality energy sources (electricity or high-temperature heat), which limits direct integration with solar or other renewable energy sources [5].

Thermal desalination using humidification-dehumidification (HDH) technology has considerable potential to reduce pressure on conventional water resources and provide reliable water supplies for arid and coastal areas. HDH systems feature simple designs and require minimal technical maintenance. The primary drawback of HDH technology is its high thermal energy demand for salt removal from seawater. As a result, integrating renewable energy sources, particularly solar energy, as an alternative to conventional energy inputs has become an increasing trend in HDH system development [6].

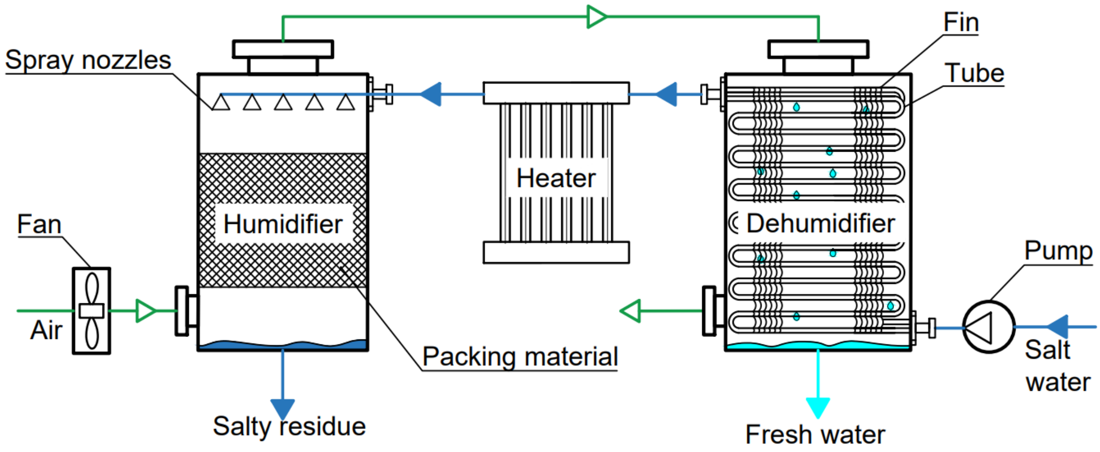

Figure 1. Desalination system working on the air humidification-dehumidification principle

The schematic diagram of a thermal desalination system based on the humidification-dehumidification (HDH) process is shown in Figure 1. In this system, saline water is pumped into the dehumidifier, where it circulates through tubes and is heated by the latent heat released from saturated air. Simultaneously, the air is dehumidified as it cools in the inter-tube space of the dehumidifier. The preheated saline water is further heated to the required temperature in a heater (typically 60 °C). Ambient air is drawn into the humidifier by a fan, where it comes into direct contact with the heated saline water, warming up and absorbing moisture. To provide efficient heat and mass transfer, the heated water can be sprayed through nozzles. A portion of the water evaporates into the air, while the remaining brine is discharged at the bottom of the humidifier. At the humidifier outlet, the air humidity can reach 100%. The saturated air is then fed to the dehumidifier, where water vapour condenses to produce freshwater. The cooled air is subsequently released into the environment.

The key components of any HDH system are two heat exchangers: the humidifier and the dehumidifier, illustrated in Figure 1. The dehumidifier's primary function is to condense moisture from the air to obtain freshwater. Most dehumidifiers use surface-type recuperative heat exchangers, either coil-based or with finned air-side surfaces, the required heat exchange surface area of the dehumidifier is determined based on the condition that all the water vapour absorbed in the humidifier must be condensed. In general, heat and mass transfer in dehumidifier is calculated using integral method, based on the American ARI-Standard 410–8, which is described in detail in [7].

The humidifier is a direct-contact heat and mass exchanger where moisture from saline water evaporates into the air. The performance of an HDH system depends on the amount of water vapour absorbed by the air in the humidifier. Therefore, improving heat and mass transfer efficiency in humidifiers is a key focus of experimental research on HDH systems. Different types of direct-contact heat exchangers used as humidifiers are illustrated in Figure 2.

A bubble column is a vertical tank filled with water, where air is delivered through openings in spiral tubes at the bottom of the column, illustrated in **Figure 3**. As air passes through these openings, bubbles form, facilitating intensive heat and mass transfer between the air and water inside the column. During this process, water evaporates, saturating the air with moisture. At the column outlet, heated, humidified air is obtained.

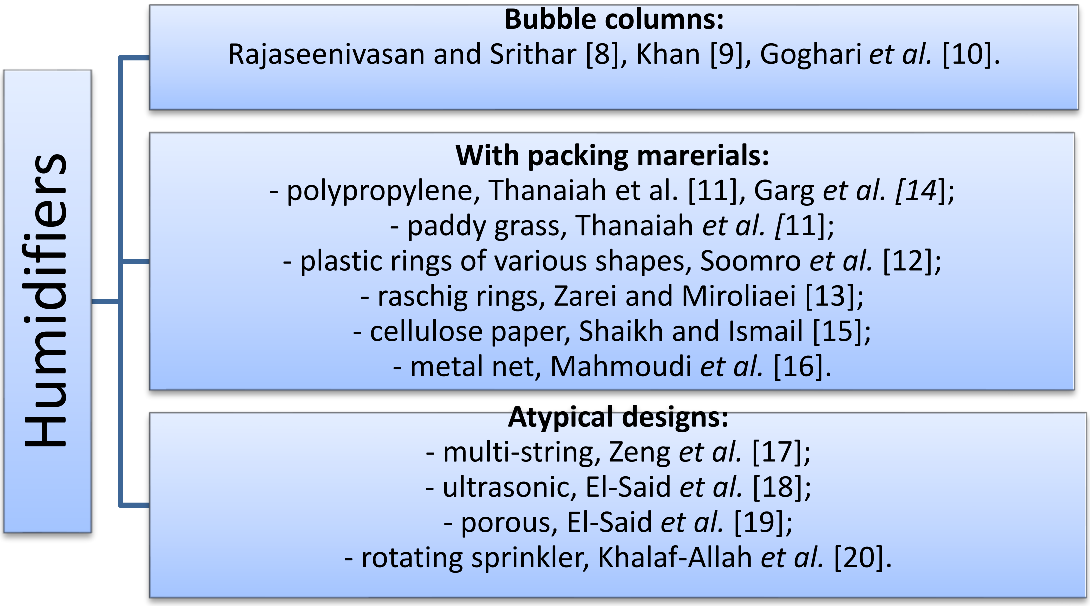

Figure 2. Types of humidifiers used in HDH systems

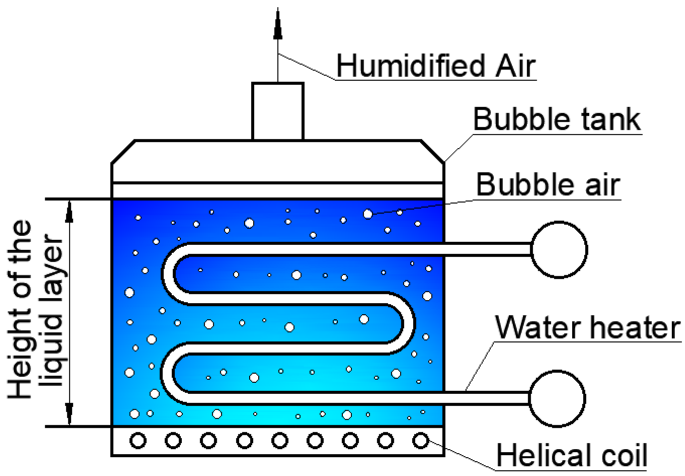

Figure 3. Bubble humidifier

Several studies have focused on evaluating the performance of bubble humidifiers. Specifically, Rajaseenivasan and Srithar [8] developed an HDH system powered by biomass. The authors found that the performance of the bubble humidifier increases with the height of the water layer, water temperature and air mass flow rate, and with the reduction of the bubble tube opening diameter. The highest fresh water production (6.1 kg/h) was observed with a bubble tube opening with a diameter of 1 mm, a water layer height of 170 mm, and a water temperature of 60 °C.

Khan *et al.* [9] experimentally determined the efficiency of the HDH system with two bubble columns. In [8], it was shown that increasing the airflow and temperature enhances the performance of the bubble columns. Additionally, optimal parameters for maximum distillate production (0.3 kg/h) were identified: input power of 0.71 kW, air temperature of 140 °C, air flow rate of 2.55 kg/h, and water levels in the first and second humidifiers of 3 cm and 6.5 cm, respectively.

Goghari *et al.* [10] experimentally investigated an HDH system featuring a two-stage bubble humidifier and a direct-contact dehumidifier. The authors determined an optimal cooling water flow rate of 2.8 L/min, which yields a maximum productivity of 3 L/h and the highest gain output ratio (GOR = 0.42). Furthermore, it was found that the humidifier efficiency exhibits a direct dependence on the air flow rate, reaching a peak value of 0.64.

Another type of humidifier is a packed-bed heat exchanger, shown in **Figure 2**. Packing elements significantly increase the contact area between water and air, ensuring efficient heat and mass transfer. Such humidifiers were studied in a series of research. Specifically, Thanaiah *et al.* [11] investigated seawater desalination using packing materials such as polypropylene and paddy grass. The steel humidifier had a square cross-section of 0.4×0.4 m and a height of 1 m. The packing density of paddy grass was 157 m^2/m^3 with a surface area of 10 m^2. The geometric characteristics of polypropylene were not provided. The maximum performance of the HDH system was 0.46 and 0.73 kg/h for polypropylene and paddy grass, respectively. At the same time, the air flow rate ranged from 20 to 170 kg/h, and the water flow rate – from 40 to 170 kg/h.

Soomro *et al.* [12] studied the properties of a hydrophobic plastic packing material of various shapes (hackettes, saddles and snowflake). The humidifier was shaped as a rectangular polycarbonate container with external dimensions of 150×150 mm^2 and a height of 320 mm. The void fraction and specific geometric surface area were 92% and 280 m^2/m^3 for hackettes; 97% and 169 m^2/m^3 for saddles; and 97% and 138 m^2/m^3 for snowflakes, respectively. During the experiments, the saline water flow rate varied between 6–18 kg/h, while the air flow rate ranged from 20 to 27 kg/h. The results did not show significant differences between the different shapes of the packing material. The performance of the HDH system was in the range of 0.25–0.6 kg/h, and the aerodynamic resistance of the humidifier amounted to 24–98 Pa/m.

Zarei and Miroliaei [13] analysed the efficiency of an HDH system with a Rushing packing. The heat exchanger had a diameter of 0.25 m and a height of 1 m. The experiments showed that the HDH system could produce up to 300 kg of freshwater per day at an inlet water temperature of 60–70 °C. The seawater flow rate was 720 kg/h, while the air flow rate was 320 kg/h.

Garg *et al.* [14] tested an HDH system with a packed-bed humidifier. The material used was a 1.1 m high layer of ABS plastic with a specific geometric surface area of 226 m^2/m^3. The authors established that the HDH system could produce 125 litres of freshwater per day at an inlet water temperature of 62 °C. Under these conditions, the optimal mass flow ratio (MR) was 2.34, and the average thermodynamic efficiency of the humidifier equalled 0.77.

Shaikh and Ismail [15] developed an HDH system based on solar collectors for the climatic conditions of India. As a packing material, the authors used 10 sheets of cellulose paper, each with a diameter of 0.4 m and a thickness of 10 cm. The humidifier was made of Plexiglas acrylic and had a cylindrical shape with a diameter of 0.4 m, and a height of 1.75 m. To ensure uniform distribution, an axial nozzle was installed 25 cm above the packing material. At an air flow rate of 10 kg/h, and a feed flow rate of 50 kg/h, the maximum productivity of the HDH system was 6.5 kg per day, while the average thermodynamic efficiency of the humidifier amounted to 0.62.

Mahmoudi *et al.* [16] experimentally investigated of a solar-powered HDH desalination system with net splash packed-bed humidifier. The results showed that for a feed saline water flow rate of 1.2 L/min and salinity of 5000 ppm, the maximum gain output ratio (GOR) was 0.24 and the specific energy consumption (SEC) was 3.48 kWh/m^3.

Packed-bed heat exchangers are highly efficient due to their large heat and mass transfer surface area and relatively low air pressure losses (10…100 Pa). However, they require substantial amounts of saline water (MR > 1). Additionally, saline water must be pumped through the humidifier at high pressure for effective nozzle spraying. As a result, the pump's power consumption increases, leading to higher SEC values.

Zeng *et al.* [17] suggested a compact humidifier design for an HDH system. The heat exchanger consists of a dense array of 24 vertical strings, along which a thin film of heated water flows down due to gravity. A counter-flow air stream contacts the liquid film and carries the generated water vapour to the dehumidifier. This configuration ensures high efficiency in heat and mass exchange processes while maintaining low air pressure drops. During the experiments, the saline water flow rate was 1.6 and 2.4 g/s, while the air flow rate varied from 1.5 to 12.5 kg/h. The saline water was heated to the temperatures of 80 and 90 °C. Under these conditions, the productivity of the string humidifier ranged from 5 to 12.5 kg/day; the thermodynamic efficiency ranged from 0.25 to 0.9, and the air pressure drop varied from 1 to 4 Pa. The advantages of the string humidifier are low aerodynamic resistance and high heat and mass transfer efficiency. However, these performance indicators are achieved at a water temperature of 90 °C. Heating water to such a high temperature is impractical due to the potential for salt deposition in the HDH system components.

The original humidifier design was presented in [18]. The authors employed high-frequency ultrasonic sprayers, achieving 100% relative humidity at the humidifier outlet. It was found that increasing the number of sprayers and air flow rate enhanced daily distillate production, with a maximum output of 7.74 kg of freshwater per day at an airflow rate of 40 kg/h. Later, El-Said *et al.* [19], modernised the humidifier by replacing ultrasonic sprayers with porous activated carbon tubes. The authors' findings confirmed that the HDH system's productivity primarily depended on the airflow rate, with a maximum daily distillate production of approximately 6.12 kg. However, the use of porous tubes did not show significant advantages over ultrasonic sprayers in terms of humidification efficiency. The energy performance of the HDH systems in both studies remained at a comparable level. Despite the complexity of the design, atypical humidifiers demonstrate performance comparable to packed-bed heat exchangers.

Khalaf-Allah *et al.* [20] developed a humidifier with a rotating sprinkler to ensure uniform spraying of saline water. The authors examined the effects of droplet slot distributions, sprinkler rotation speed, and air and water flow rates on the performance of the HDH system. The results indicate that a higher number of slots in the sprinkler reduces productivity, whereas increasing the sprinkler's rotation speed enhances distillate production. The maximum freshwater output of 1.6 kg/h was achieved at the highest air (160 kg/h) and water (184 kg/h) flow rates. Furthermore, humidifier with rotating sprinkler consume more electricity.

According to these reviews, the most common types of humidifiers in HDH systems are packed-bed heat exchangers and bubble column humidifiers. Bubble column humidifiers demonstrate the highest thermodynamic efficiency; however, they also exhibit significant aerodynamic resistance (exceeding 10 kPa) and low volumetric productivity. These factors contribute to an increase in the system's specific energy consumption (*SEC*).

The lack of data on pressure losses in both water and air complicates a comprehensive analysis of existing humidifier designs, making it impossible to determine their economic and exergy efficiency. This prompts further research to find optimal humidifier designs.

In the present study, it is proposed to use a vertical tube as a humidifier, where the internal volume serves as the active heat and mass transfer zone during the evaporation of moisture from water to air. The optimal operating parameters of the film-type humidifier have been experimentally determined to achieve maximum productivity and energy efficiency. A comparison of the efficiency of the film direct contact heat exchanger with other types of humidifiers has been conducted.

EXPERIMENTAL SETUP, PROCEDURE AND CONDITIONS

The schematic diagram of the experimental setup is shown in **Figure 4**. The setup has an open-air circuit and a closed-water circuit. Its main components include humidifier (10), water heater (6), pump (8), fan (15), and a control and measurement system for the required parameters.

System Operation

The experimental setup operates as follows. Humidifier (10) is a transparent acrylic tube, 2 m long with an inner diameter of 26 mm, fixed between two reservoirs. The upper reservoir is filled with water using pump (8), ensuring a uniform liquid film flow along the inner surface of humidifier (10). Water from the tube flows down into the lower reservoir. The water level in the lower reservoir is controlled using piezometer (12). From the lower reservoir, the water is pumped back to the upper reservoir by diaphragm pump (8), completing a full cycle. The water flow rate is smoothly adjusted using a laboratory power supply unit (9) by varying the input current (0-6 A) and voltage (0–24 V) supplied to the pump. To heat the water to the required temperature, a flow-through electric heater 6 is used. The required power of the heater is set by regulator (5).

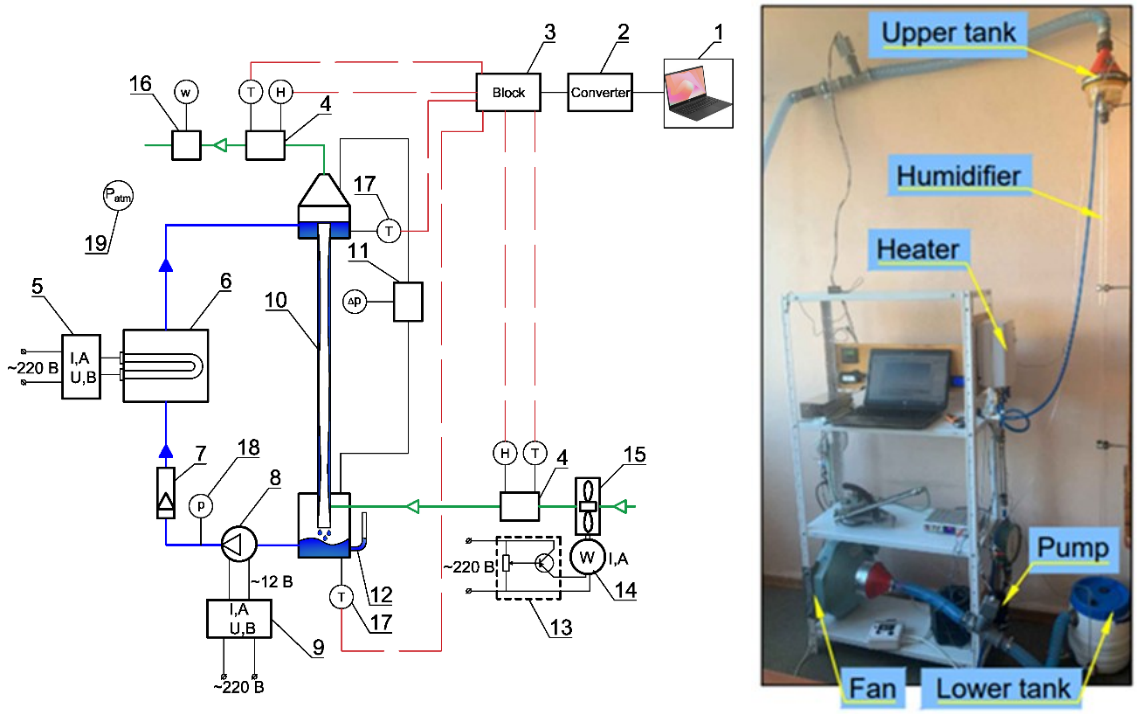

Figure 4. Schematic and the photo of the experimental setup

As shown in **Figure 4**, the experimental setup comprises a laptop (1), an RS485/USB interface converter (2), an eight-channel meter (3), an air temperature and relative humidity converter (4), a power regulator with a temperature sensor (5), a flow-through water heater (6), a rotameter (7), a diaphragm pump (8), a laboratory power supply unit with smooth adjustment of output parameters using current and voltage potentiometers (0–24 V, 6 A) and a digital electronic meter (9), an experimental humidifier (10), an inclined tube micromanometer (11), a piezometer (12), an adjustable laboratory autotransformer (13), a digital multifunction AC meter (14), a fan (15), an anemometer (16), and a Pt1000 temperature sensor (17).

Air from the surrounding environment is supplied to humidifier (10) through the lower reservoir by fan (15), rises upwards, and exits into the environment from the upper reservoir. During heat and mass exchange between the air and the falling liquid film inside the tube, the air is heated and humidified, while the water is cooled. The air velocity inside the humidifier is adjusted by varying the input voltage of the fan within the range of 0–220 V using autotransformer (13). The power consumption of the fan is measured using a digital multifunction AC meter (14).

Air from the surrounding environment is supplied to humidifier (10) through the lower reservoir by fan (15), rises upwards, and exits into the environment from the upper reservoir. During heat and mass exchange between the air and the falling liquid film inside the tube, the air is heated and humidified, while the water is cooled. The air velocity inside the humidifier is adjusted by varying the input voltage of the fan within the range of 0–220 V using autotransformer (13). The power consumption of the fan is measured using a digital multifunction AC meter (14).

To determine the potential effect of salt deposition on the heat and mass transfer processes in the film humidifier, preliminary experiments were conducted using an aqueous NaCl (sodium chloride) solution with a concentration of 35 g/L, which simulates typical seawater conditions. The obtained results demonstrated no noticeable change in the heat and mass transfer rates at this concentration level, and no significant brine accumulations were observed at the bottom of the lower tank. Consequently, all subsequent experiments were performed using brackish water.

Measuring System

To measure the required parameters, the following instruments were integrated into the experimental setup. Rotameter (7) was connected to the water circuit to measure the volumetric flow rate of water. The pump head was measured using a manometer. The air velocity at the humidifier outlet was measured with anemometer (16). The total air pressure drop in the humidifier was recorded using micromanometer 11. The air temperature and relative humidity at the inlet and outlet of the humidifier were measured using thermocouples (17). The air temperature and relative humidity at the inlet and outlet of the humidifier were measured using digital converters (4). All temperature and relative humidity values were transmitted in real time to a laptop via a sequentially installed eight-channel meter (3) and interface converter (2). Atmospheric pressure was measured with a barometer. The specifications and measurement uncertainties for all instruments are shown in **Table 1**. The range of changing operating conditions is shown in **Table 2**.

Table 1. Specifications of measuring instruments

Position	Instrument	Parameter	Range	Accuracy
4	Digital Converter DVT-303	Air temperature Air relative humidity	−35–80 °C 0–100%	±0.4 °C ±3%
17	Thermocouple Pt1000	Water temperature	−40–270 °C	±(0.3+0.005t) °C
7	Rotameter	Water flow rate	up to 100 L/h	±1 L/h
16	Anemometer testo 410i	Air velocity	0.4–30 m/s	±0.2 m/s ±2%
11	Micromanometer	Air pressure drop	up to 600 Pa	± 3 Pa
18	Manometer	Pump head	up to 60 kPa	±0.6 kPa
19	Barometer	Atmospheric pressure	80–106 kPa	±0.2 kPa
5	Single channel output DC power supply	Heater power	0–30 A 50–300 V	±0.01 A ±0.1 V
9,14	Digital multi-function meter	Fan power Pump power	up to 4.5 kW	±1%

Table 2. Measured experimental variables

Parameter	Range	Standard Uncertainty
Air velocity in the tube	3.3–15.2 m/s	3.3–8%
Mass flow rate of water	10–80 kg/h	3.1–9.6%
Air pressure drop in the humidifier	19–324 Pa	1–15%
Air temperature at the humidifier inlet	24–29 °C	2%
Air humidity at the humidifier inlet	≈65%	4.7%
Air temperature at the humidifier outlet	27–48 °C	2%

Parameter	Range	Standard Uncertainty
Air humidity at the humidifier outlet	≈98%	3%
Water temperature at the humidifier inlet	28–59 °C	1.3%
Water temperature at the humidifier outlet	25–42 °C	1.4%
Pump head	22.3 kPa	2.7%
Power consumption of the fan	≈7.5 W	1%
Power consumption of the pump	≈1.5 W	1%

Data Reduction

The data processing of the measured results follows the procedures outlined below. The thermodynamic properties of water and humid air are determined using the CoolProp library [21].

The mass flow rate of air at the inlet of the experimental setup is measured using the formula:

$$m_{\mathrm{a}} = 0.25\pi w_{\mathrm{a}} d^2 \rho_{\mathrm{a,in}}. \tag{1}$$

The liquid velocity is calculated by the formula:

$$w_{\mathrm{w}} = \frac{4m_{\mathrm{w}}}{\pi d^2 \rho_{\mathrm{w,in}}}. \tag{2}$$

The heat balance of the experimental humidifier can be calculated as follows:

$$Q_{\mathrm{a}} = Q_{\mathrm{w}}. \tag{3}$$

The heat supplied to the water in the flow-through heater (6), that shown in Figure 4 is determined using the formula:

$$Q_{\mathrm{w}} = m_{\mathrm{w}} c_{p,\mathrm{w,in}} t_{\mathrm{w,in}} - (m_w - \Delta\omega) c_{p,\mathrm{w,out}} t_{\mathrm{w,out}}, \tag{4}$$

where $\Delta\omega$ denotes the humidifier performance (the mass flow rate of moisture transferred from hot water to the air) and is calculated as follows:

$$\Delta\omega = m_{\mathrm{a}}(\omega_{\mathrm{out}} - \omega_{\mathrm{in}}). \tag{5}$$

The total heat transferred to the air in the humidifier can be calculated as follows:

$$Q_{\mathrm{a}} = (m_{\mathrm{a}} + \Delta\omega) h_{\mathrm{a,out}} - m_{\mathrm{a}} h_{\mathrm{a,in}}. \tag{6}$$

The variation between Q_{a} and Q_{w} for all the tests is within 8%.

The electric energy consumption of the pump and fan to transmit one kg of moisture to the air is measured as follows:

$$SEC = (N_{\mathrm{fan}} + N_{\mathrm{pump}})/\Delta\omega. \tag{7}$$

The evaporation rate per unit humidifier volume is calculated using the formula:

$$ER = \Delta\omega / V_{\text{hum}}, \tag{8}$$

$$V_{\text{hum}} = 0.25\pi d^2 l. \tag{9}$$

The humidifier efficiency is calculated as follows:

$$\eta_{\text{hum}} = \max\left(\eta_{\text{hum,a}}; \eta_{\text{hum,w}}\right), \tag{10}$$

where $\eta_{\text{hum,a}}$ is the humidifier efficiency based on air:

$$\eta_{\text{hum,a}} = \frac{h_{\text{a,out}} - h_{\text{a,in}}}{h_{\text{a,out}}^{\text{id}} - h_{\text{a,in}}}. \tag{11}$$

$\eta_{\text{hum,w}}$ is the humidifier efficiency based on water:

$$\eta_{\text{hum,w}} = \frac{h_{\text{w,in}} - h_{\text{w,out}}}{h_{\text{w,in}} - h_{\text{w,out}}^{\text{id}}}. \tag{12}$$

The eq. (11) and eq. (12) $h_{\text{a,out}}^{\text{id}}$ provide the ideal enthalpy of air at the outlet of the humidifier under the condition of full air saturation, φ_{out}=100% and $t_{\text{a,out}} = t_{\text{w,in}}$ $h_{\text{w,out}}^{\text{id}}$ is the ideal enthalpy of water at the outlet of the humidifier (under the condition $t_{\text{w,out}} = t_{\text{a,in}}$).

The exergy efficiency of the humidifier is calculated using the formula [22]:

$$\varepsilon_{\text{hum}} = \frac{E_{\text{P}}}{E_{\text{F}}} = \frac{E_{\text{a,out}} + E_{\text{a,in}}}{E_{\text{w,in}} + E_{\text{w,out}}}, \tag{13}$$

where E_{P} is the exergy of the "product" or the increase in exergy between the inlet and outlet for continuous air flow; E_{F} is the exergy of the "fuel" or the decrease in exergy between the inlet and outlet for the material flow of water; $E_{\text{a,in}}$ 0 W is the air exergy at the inlet to the humidifier (the exergy of the surrounding environment). The values of other components in eq. (13) are determined by the formulae from [23].

Exergy of the humidified air at the humidifier outlet:

$$\begin{aligned} E_{\text{a,out}} = m_{\text{a}} \Bigg\{ & \left(c_{p\text{.a,out}} + \omega_{\text{a,out}} c_{p\text{.v}}\right) \times \left(T_{\text{a,out}} - T_{\text{a,in}} - T_{\text{a,in}} \ln\frac{T_{\text{a,out}}}{T_{\text{a,in}}}\right) \\ & + R_{\text{a}} T_{\text{a,in}} \left[\left(1 + \frac{M_{\text{a}}}{M_{\text{v}}}\omega_{\text{a,out}}\right) \ln\frac{1 + \frac{M_{\text{a}}}{M_{\text{v}}}\omega_{\text{a,in}}}{1 + \frac{M_{\text{a}}}{M_{\text{v}}}\omega_{\text{a,out}}} + \frac{M_{\text{a}}}{M_{\text{v}}}\omega_{\text{a,out}} \ln\frac{\omega_{\text{a,out}}}{\omega_{\text{a,in}}}\right]\Bigg\}. \end{aligned} \tag{14}$$

Exergy of water at the inlet to the humidifier:

$$E_{\mathrm{w,in}} = m_{\mathrm{w}} \left[h_{\mathrm{w,in}} - h_{\mathrm{w,out}}^{\mathrm{id}} - T_{\mathrm{a,in}} \left(s_{\mathrm{w,in}} - s_{\mathrm{w}}^{\mathrm{id}} \right) - R_{\mathrm{v}} T_{\mathrm{a,in}} \ln \frac{\varphi_{\mathrm{a,in}}}{100} \right], \tag{15}$$

where $s_{\mathrm{w}}^{\mathrm{id}}$ is the "dead state" entropy, J/kgK.

Exergy of water at the outlet of the humidifier:

$$E_{\mathrm{w,out}} = (m_{\mathrm{w}} - \Delta\omega) \left[h_{\mathrm{w,out}} - h_{\mathrm{w,out}}^{\mathrm{id}} - T_{\mathrm{a,in}} \left(s_{\mathrm{w,out}} - s_{\mathrm{w}}^{\mathrm{id}} \right) - R_{\mathrm{v}} T_{\mathrm{a,in}} \ln \frac{\varphi_{\mathrm{a,in}}}{100} \right]. \tag{16}$$

Uncertainty reduction

In this study, the experimental uncertainty is evaluated using the method described by Holman *et al.* [24]. In the case when R is a function of independent variables X_1, X_2, X_3, …, X_n, i.e.:

$$R = f(X_1, X_2, X_3, \dots \dots, X_{\mathrm{n}}). \tag{17}$$

the uncertainty of the R parameter can be calculated using the equation:

$$\Delta R = \sqrt{\left(\frac{\partial R}{\partial X_1}\Delta_1\right)^2 + \left(\frac{\partial R}{\partial X_2}\Delta_2\right)^2 + \left(\frac{\partial R}{\partial X_3}\Delta_3\right)^2 + \dots + \left(\frac{\partial R}{\partial X_n}\Delta_n\right)^2}, \tag{18}$$

where Δ_1, Δ_2, Δ_3, …, Δ_n are the uncertainties of independent variables X_1, X_2, X_3, …, X_n.

The relative uncertainty (U_R) is calculated as follows:

$$U_R = \frac{\Delta R}{R} 100\% \,. \tag{19}$$

Eq. (18) is used to estimate the uncertainties associated with all the calculated parameters. The final calculation results are presented in **Table 3**. It can be concluded that the maximum overall uncertainty of the experimental results is ±11%.

Table 3. The standard uncertainties of calculated parameters

Parameter	Range	Uncertainty
m_{a}	7.4−35 kg/h	3.4−7.1 %
w_{w}	0.005−0.042 m/s	3.2−9.6 %
$\Delta\omega$	114−682 g/h	6.9%
Q_{a}	89−557 W	11%
Q_{w}	90−554 W	8.4%
SEC	0.013−0.081 kWh/kg	7.1%
ER	108−642 kg/m³h	6.9%
η_{hum}	0.52−0.89	3.7%
$\varepsilon_{\mathrm{hum}}$	0.32−0.66	5.3%

RESULTS AND DISCUSSION

This section presents the experimental results and provides a detailed discussion of the performance indicators of the proposed film humidifier. To determine the optimal operating conditions, the influence of various operational parameters, such as air flow rate, water flow rate and supplied heat, on the overall system performance was systematically evaluated.

Optimal Air Flow Rate

It is known that the higher the air flow rate passing through an HDH system, the greater its productivity [20]. This is because an increase in airflow rate intensifies heat and mass transfer processes in the humidifier. As a result, more moisture is transferred to the air in the heat exchanger. At the same time, when the air flow rate increases in vertical tube direct contact heat exchangers, the liquid film flow is disrupted, and simultaneous upward movement of water and air begins. This regime is called "flooding" and is characterized by the detachment and entrainment of water bubbles by the air flow, along with a sudden increase in hydraulic resistance [25]. Operating an HDH system under such conditions will lead to distillate contamination and increased energy consumption. Experimental data provided by various authors indicate that the onset limits of the flooding regime are quite ambiguous, and existing flooding correlations show significant discrepancies among them [26].

Thus when using a vertical tube as a humidifier, it is necessary to find an optimal air flow rate that, on the one hand, ensures maximum HDH system productivity and, on the other, prevents the onset of an inefficient flooding regime. To achieve this goal, a number of experiments were conducted, measuring the total air pressure losses in the humidifier at different air velocities and water flow rates. The obtained results are shown in Figure 5.

As seen from Figure 5, the experimental values of the total air pressure drop of single-phase flow ($m_{\mathrm{w}} = 0$ kg/h) almost coincide (error ± 14%) with the frictional pressure drop obtained with the following Darcy–Weibach's correlation:

$$\Delta P_{\mathrm{a,calc}} = 0.5 f d^{-1} \rho_{\mathrm{a,in}} w_{\mathrm{a,in}}^{2}, \tag{20}$$

$$f = 0.3164 Re_{\mathrm{a}}^{-0,25}. \tag{21}$$

For the air in the tube humidifier, the friction pressure loss is dominant. For engineering calculations, the values of the hydrostatic pressure difference and the acceleration pressure loss can be neglected.

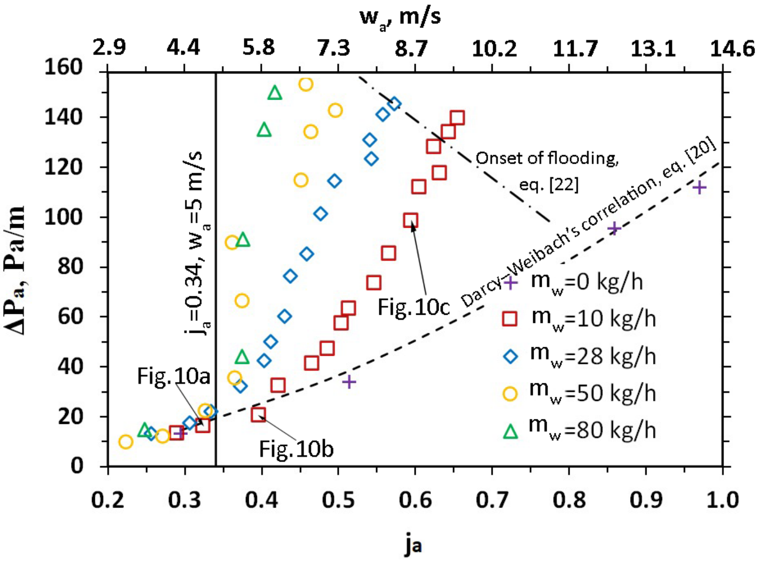

Figure 5. Experimental values of total air pressure drop in a tube humidifier

The identification of the onset of the flooding regime was conducted under the condition of equality between the superficial phase velocities of water and air [27]:

$$j_a^{1/2} = -0.439 j_w - 0.123 j_w^{1/2} + 0.791, \tag{22}$$

where superficial phase velocities are determined as follows:

$$j_i = w_i \left[\frac{\rho_{i,in}}{(\rho_{w,in} - \rho_{a.in}) dg} \right]^{\frac{1}{2}}. \tag{23}$$

The index $i = a$, w denotes air and liquid phase.

At an air velocity in the tube of less than 5 m/s (j_a<0.34), regardless of the water flow, the total air pressure drop is equal to the pressure losses of a single-phase flow. Under these parameters, the liquid film flows down almost without waves and does not interfere with the movement of air (**Figure 6a**). As the air velocity increases further, the total air pressure drop rises much faster than in a single-phase flow and, at water flow rates above 50 kg/h, becomes almost independent of the air flow rate. This is due to the increasing amplitude and wave frequency on the liquid film surface. Additionally, the air begins to entrain water from the wave crests in the surrounding area of the tube outlet. The first appearance of single droplets from the wavy film surface is observed at w_a=6.18 m/s and j_a=0.42 (**Figure 6b**). The droplets rise with the air flow to a small height and then fall back down under the influence of gravity.

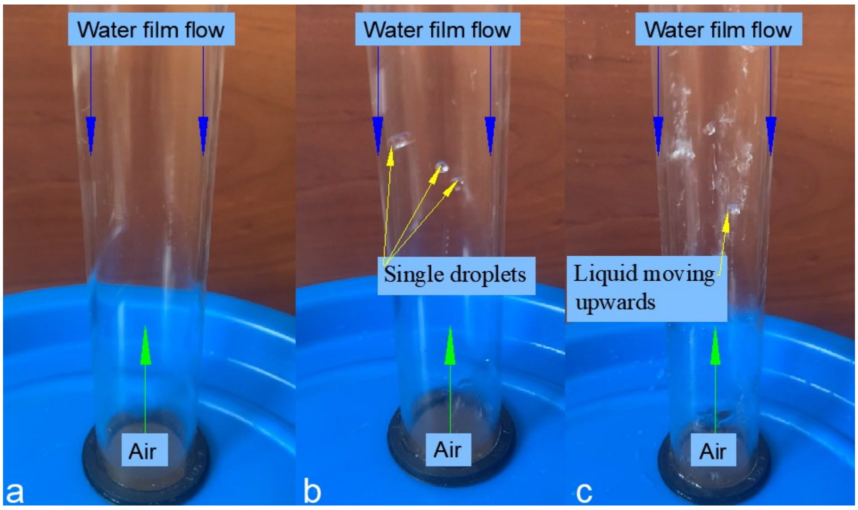

Figure 6. Flow regimes in a tube humidifier

At a water flow rate of 10 kg/h, the onset of the flooding regime is observed at j_a=0.61 (w_a=8.83 m/s, Re_a=15254). Under these conditions, most of the liquid flowing to the lower edge of the tube is entrained by the incoming atmospheric air and recirculated back into the humidifier. As a result, a liquid layer forms at the bottom of the tube, through which the air passes, leading to the flow flooding (**Figure 6c**). It should be noted that the experimentally obtained values of Re_a, corresponding to the onset of transition between flow regimes, align with those reported in the study **[25]**.

From **Figure 7**, it is evident that limiting the maximum air flow rate based on the onset of the flooding regime is impractical, as a sharp increase in the total air pressure drop (and consequently in fan power consumption) begins at lower air velocities. Considering this, it is proposed to limit the maximum superficial phase velocity in the humidifier to 0.34. Under this condition, contamination of the condensate by droplets from saline water is prevented, and the lowest pressure losses are ensured.

Optimal Mass Flow Rate Ratio

The mass flow rate ratio (*MR*) is one of the key indicators for evaluating the energy efficiency of an HDH system. The *MR* value is calculated as the ratio between the saline water flow rate and the external air flow rate:

$$MR = m_{\mathrm{w}}/m_{\mathrm{a}}. \tag{24}$$

It is established that the lower the *MR* value, the higher the energy efficiency of the HDH system [28]. This is because a lower saline water flow rate through the dehumidifier results in a higher outlet temperature of the water Figure 1. Consequently, less heat is required in the heater to raise the water to the desired temperature. However, for vertical tubes, the minimum water flow rate is determined by maintaining a continuous falling film over the entire surface of the tube [29].

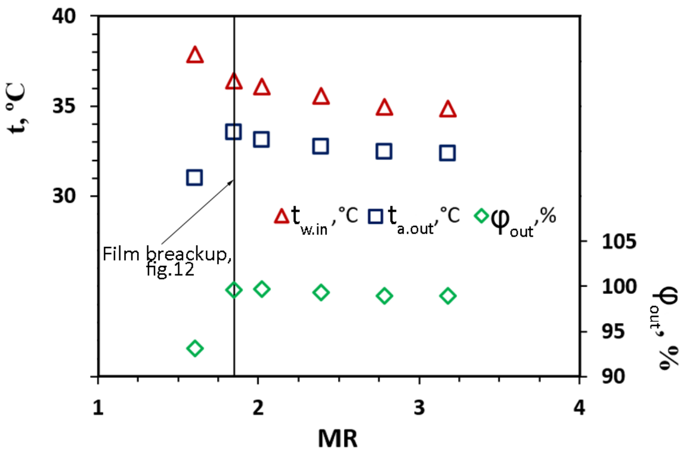

Figure 7. Mass flow rate ratios required to maintain continuous falling film

As seen from Figure 7, the temperatures $t_{\mathrm{w.in}}$ and $t_{\mathrm{a.out}}$ increase as *MR* decreases, while the humidity value φ_{out} remains constant. When the film break-up occurs (Figure 8), the temperature $t_{\mathrm{w.in}}$ continues to rise, whereas the values $t_{\mathrm{a.out}}$ and φ_{out} drop sharply. This is because the disruption of the continuous falling film reduces the intensity of the heat and mass transfer process in the tube. As a result, the amount of heat transferred to the air in the humidifier decreases.

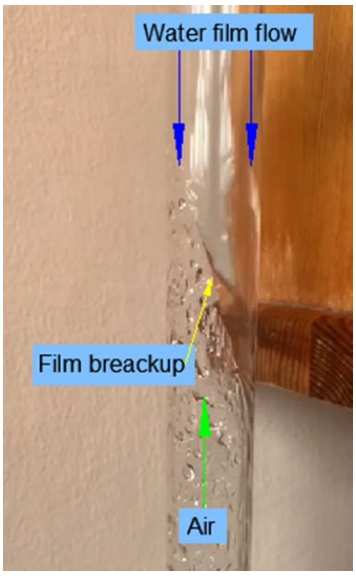

Figure 8. The onset of the film break up at MR=2

The analysis of **Figure 9** shows that reducing the water flow rate (and consequently the *MR* coefficient) leads to an overall increase in the humidifier efficiency. Specifically, the mass flow rate of moisture $\Delta\omega$ increases, the specific energy consumption (*SEC*) decreases, while the thermodynamic and exergy efficiency of the humidifier remain nearly unchanged. However, when the film break-up occurs (**Figure 8**, Video 4), *SEC* sharply increases, while $\Delta\omega$, ε_{hum}, η_{hum} decrease significantly. This operating mode is inefficient for an HDH system. Therefore, setting the minimum *MR* coefficient for tube humidifiers at 2 is a reasonable approach. Under these conditions, continuous liquid film flow is maintained, ensuring the most efficient humidifier performance.

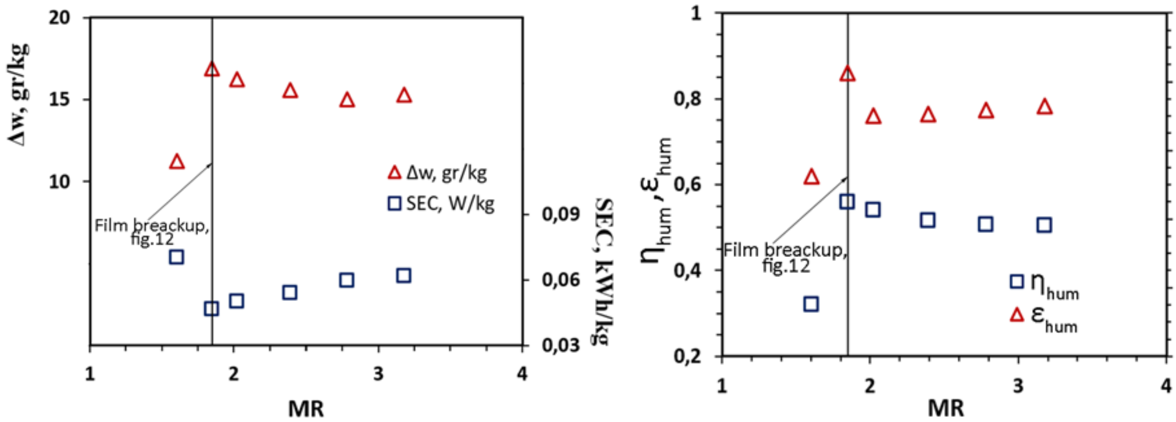

Figure 9. Impact of MR on the humidifier's energy efficiency indicators

Energy Efficiency Indicators

A series of studies was conducted to determine the maximum energy efficiency of a tube humidifier. All experiments were carried out at a constant (optimal) air velocity and water flow rate (w_a = 5 m/s, m_a = 11 kg/h, MR = 2). During the experiments, the inlet water temperature at the inlet of the humidifier $t_{w.in}$ was varied. The maximum $t_{w.in}$ value was limited to 60 °C to prevent scale formation in the system components **[6]**. The required $t_{w.in}$ value was set by adjusting the power Q_w of water flow heater (6) using regulator (5), shown in **Figure 4**.

The effect of $t_{w.in}$ on the energy performance of a tube humidifier is considered next. As seen from **Figure 10**, the higher the $t_{w.in}$ in value, the higher the outlet air temperature $t_{a.out}$. This enhances heat and mass transfer processes in the humidifier and consequently increases its performance as shown in **Figure 11**. At the same time, the specific energy consumption of the humidifier remains nearly unchanged.

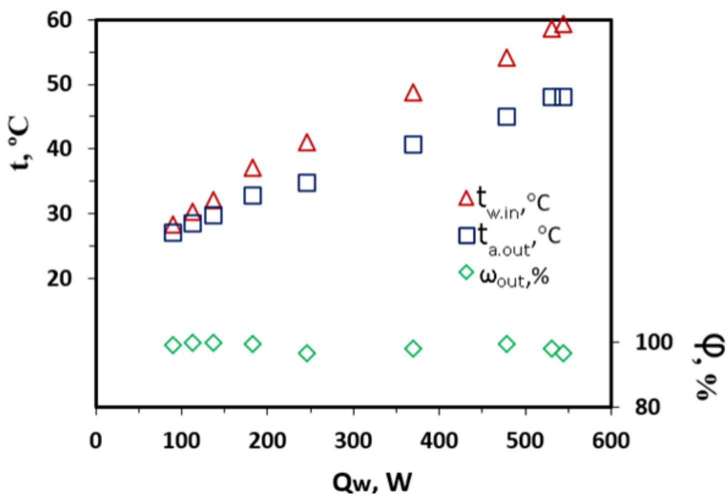

Figure 10. Impact of the supplied heat on air and water parameters

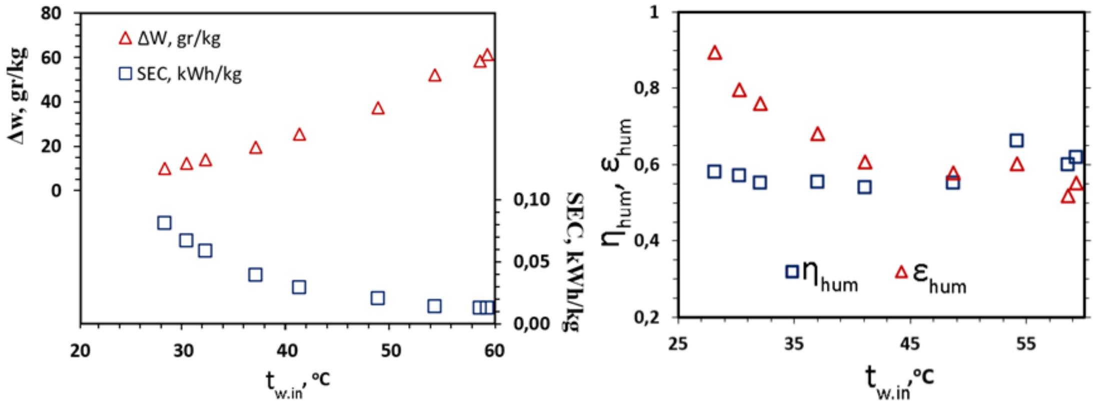

Figure 11. Impact of the supplied heat on the energy efficiency of the humidifier

As seen from **Figure 11**, the thermodynamic efficiency η_{hum} decreases with an increase in $t_{\mathrm{w.in}}$. This is due to the growing temperature difference ($t_{\mathrm{w.in}} - t_{\mathrm{a.out}}$) in the upper part of the humidifier. According to eq. (10), as this temperature difference ($t_{\mathrm{w.in}} - t_{\mathrm{a.out}}$) increases, the irreversibility of heat and mass transfer processes in the humidifier also rises. At the same time, the exergy efficiency $\varepsilon_{\mathrm{hum}}$ remains practically unchanged, with an average value of 0.58.

THERMODYNAMIC MODEL AND CALCULATION METHOD

Based on the experimental data obtained in sections "**Optimal air flow rate**" and "**Optimal MR ratio**", the thermodynamic model of a tube humidifier was developed using the engineering software PTC Mathcad. The model includes balance eq. (4) and eq. (6) and the amount of heat transferred from the heated water to the air in the humidifier due to heat and mass transfer **[25]**:

$$Q_{\mathrm{hmt}} = Q_{\mathrm{evap}} + Q_{\mathrm{con}} = \Delta\omega h_{\mathrm{vl}} + h_{\mathrm{con}} F_{\mathrm{hum}} \Delta T, \tag{25}$$

where Q_{evap} is the heat transferred by water evaporation into the air (W); Q_{con} is the heat transferred to the air due to its heating (W).

The amount of moisture absorbed by the air is determined using the following equation:

$$\Delta\omega = J F_{\mathrm{hum}}. \tag{26}$$

The diffusion flux is calculated using the formula:

$$J = \frac{h_{\mathrm{d}}}{R_{\mathrm{v}} t_{\mathrm{a.aver}}} \left(p_{\mathrm{w,par}} - p_{\mathrm{a,par}}\right). \tag{27}$$

The partial pressure of water vapour in moist air along the interphase surface $p_{\mathrm{w.par}}$ is determined based on the average water temperature. The partial pressure of water vapour in the moist air away from the interphase surface $p_{\mathrm{a.par}}$ is assumed to be the arithmetic mean of partial pressures at the air inlet and outlet of the humidifier:

$$p_{\mathrm{a,par}} = 0.5\left(p_{\mathrm{a,in,par}} + p_{\mathrm{a,out,par}}\right). \tag{28}$$

The pressures $p_{\mathrm{a,in,par}}$ and $p_{\mathrm{a,out,par}}$ are determined by the temperatures $t_{\mathrm{a,in}}$ and $t_{\mathrm{a,out}}$, respectively.

The correlations for determining the heat and mass transfer coefficients are derived from [25]:

$$h_{\mathrm{d}} = ShD/d, \tag{29}$$

$$h_{\mathrm{con}} = Nu\lambda/d, \tag{30}$$

where:

$$Sh = 0.009Re_{\mathrm{a}}^{0.8}Re_{\mathrm{f}}^{0.16}Sc_{\mathrm{a}}^{0.4}, \tag{31}$$

$$Nu = 0.009Re_{\mathrm{a}}^{0.8}Re_{\mathrm{f}}^{0.16}Pr_{\mathrm{a}}^{0.4}. \tag{32}$$

The experimental results indicate that the tube humidifier operates most efficiently at a constant air velocity (j_{a}=0.34, section – **Optimal air flow rate**), and a constant water flow rate (MR=2, Section – **Optimal MR ratio**). Additionally, the operational temperature range for air and water in HDH systems varies between 20–60 °C [30]. This allows for assuming constant values of w_{a}, MR, v_{a}, Sc_{a}, and D, and by substituting them into eq. (29) and eq. (30), a simplified empirical formula for engineering calculations is obtained:

$$h_{\mathrm{d}} = 0.0246d^{-0.04}, \tag{33}$$

$$h_{\mathrm{con}} = 26d^{-0.04}. \tag{34}$$

The model validation was carried out by comparing the experimental and calculated values of air and water temperatures at the humidifier outlet. As seen from Figure 12, all the temperatures align with an accuracy of ±4. The only exception is the point at which the film break-up occurs. Under these conditions, the mathematical model cannot be applied.

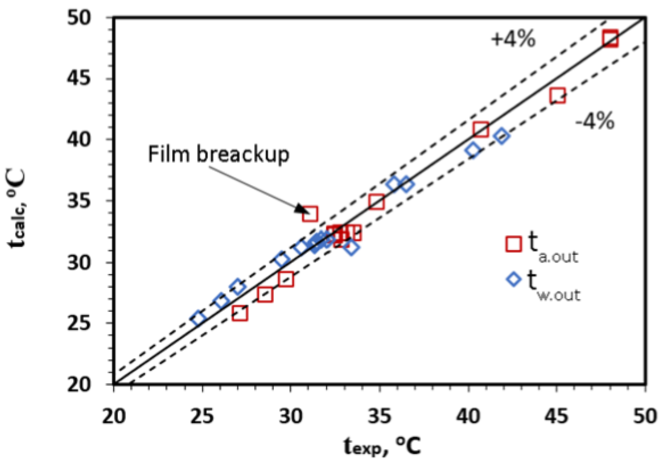

Figure 12. Validation of the thermodynamic model with experimental data

The calculation algorithm for a tube humidifier is shown in Figure 13. The following input data were used for humidifier modelling:

- water inlet temperature $t_{\mathrm{w,in}}$ = 60 °C;
- constant air velocity and water flow rate: j_{a} = 0.34, MR=2;
- external air parameters $t_{\mathrm{a,in}}$ = 25 °C, $\varphi_{\mathrm{a,in}}$ = 50%;
- air humidity at the humidifier outlet $\varphi_{\mathrm{a,out}}$ = 98%.

The modelling results provide the values $t_{a,out}$ and $t_{w,out}$ for different geometric dimensions of the humidifier. Based on these results, the following energy characteristics of the humidifier are determined: $\Delta\omega$, ER, ε_{hum}, η_{hum}.

As seen from **Figure 14**, the larger the values of d and h, the more moisture will be absorbed by the air. A larger diameter allows more air to pass through, and a higher tube improves the heat and mass transfer efficiency. However, with large diameters (d > 50 mm), the air volume passing through the central part of the tube may not reach saturation due to insufficient contact area with the water and limited interaction time. Under these conditions, eq. (29) to eq. (34) start to give inaccurate results and require refinement [31].

With constant m_a, m_w, $t_{w.in}$, a larger tube height (and consequently F_{hum}) leads to a higher air temperature $t_{a.out}$. As a result, the ability of air to retain moisture increases. When the tube height exceeds 3 m, boundary conditions change. Specifically, the air velocity at which water is captured from the wave crests changes, as well as the water flow rate at which the film breaks. Under these conditions, the boundary values j_a = 0.34 and MR=2 need to be refined.

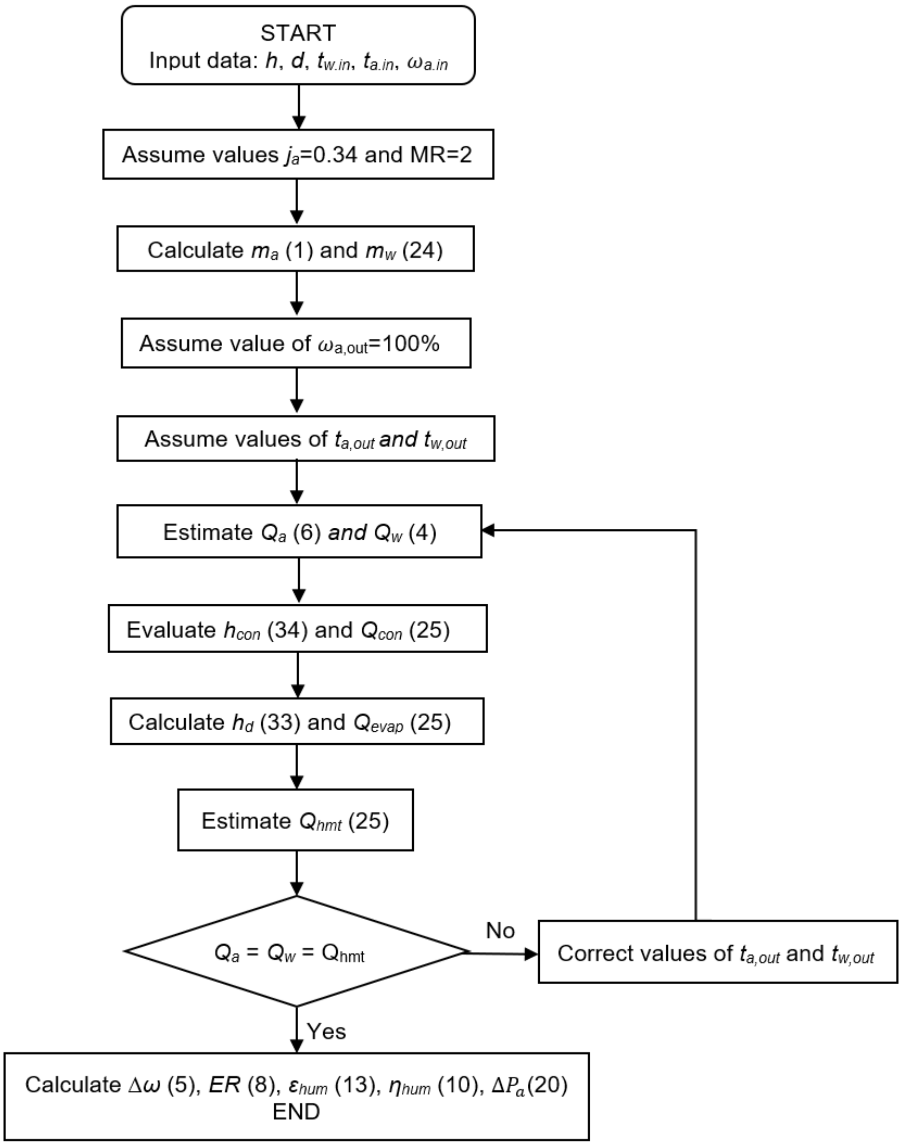

Figure 13. Algorithm for calculating the tube humidifier performance parameters

As seen from **Figure 15**, the influence of the humidifier's geometric dimensions on ε_{hum}, and η_{hum} is similar. As the diameter d increases, both indicators decrease, while an increase in the tube length l results in their growth.

Thus, the optimal dimensions of the humidifier are d = 40–50 mm and l = 2–3 m. With these parameters, the productivity of a single tube is 2–3 kg/h, the average *ER* value is 620 kg/m^{3}h, and the values ε_{hum} and η_{hum} approach 0.5–0.6.

It should be noted that the developed mathematical model is only applicable under the following conditions:

- the tube material is transparent acrylic;
- the inner diameter of the tube can be selected in the range of 20–45 mm [30];.
- the tube height should not exceed 2 m.

In other cases, the mathematical model needs to be refined.

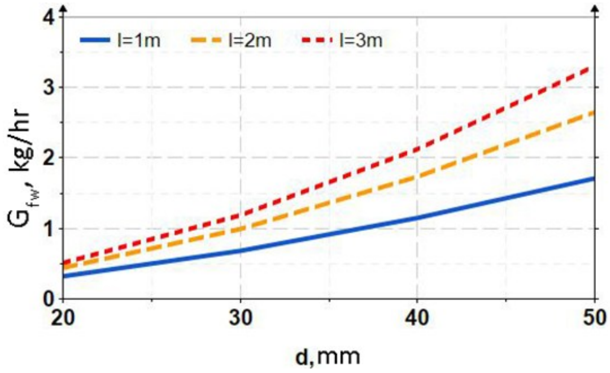

Figure 14. Impact of geometric parameters on the humidifier performance

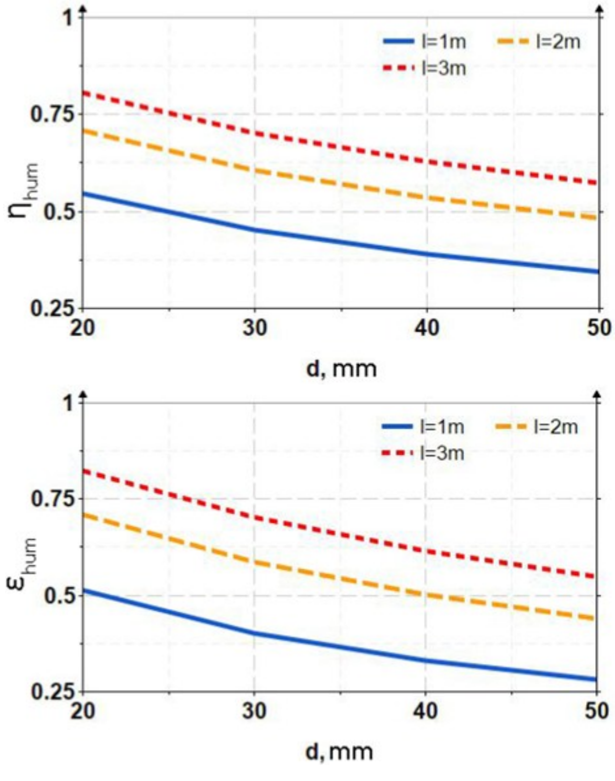

Figure 15. Impact of geometric parameters on the humidifier efficiency

HUMIDIFIERS PERFORMANCE COMPARISON

Finally, the performance metrics of the proposed film humidifier were compared with those of other types of humidifiers reported in previous studies. For comparison, the experiments were selected where the water temperature, air temperature, and mass flow rate ratios were approximately the same. Figure 16 shows that the proposed film humidifier has higher *ER* values (more than 500 kg/m³h). The *ER* values of the multi-string humidifier [17] are 2 times lower than maximum experimental *ER* across the entire *MR* range. The bubble column [8] have slightly lower (in 1.5 times) *ER* values. However, the *MR* values are 2 times greater. Humidifiers with plastic packing materials [12] and raschig rings [13] have *ER* values around 100 kg/m³h). Humidifiers with porous activated carbon tube [19] and rotating sprinkler [20] show the lowest *ER* values, which do not exceed 10 kg/m³h.

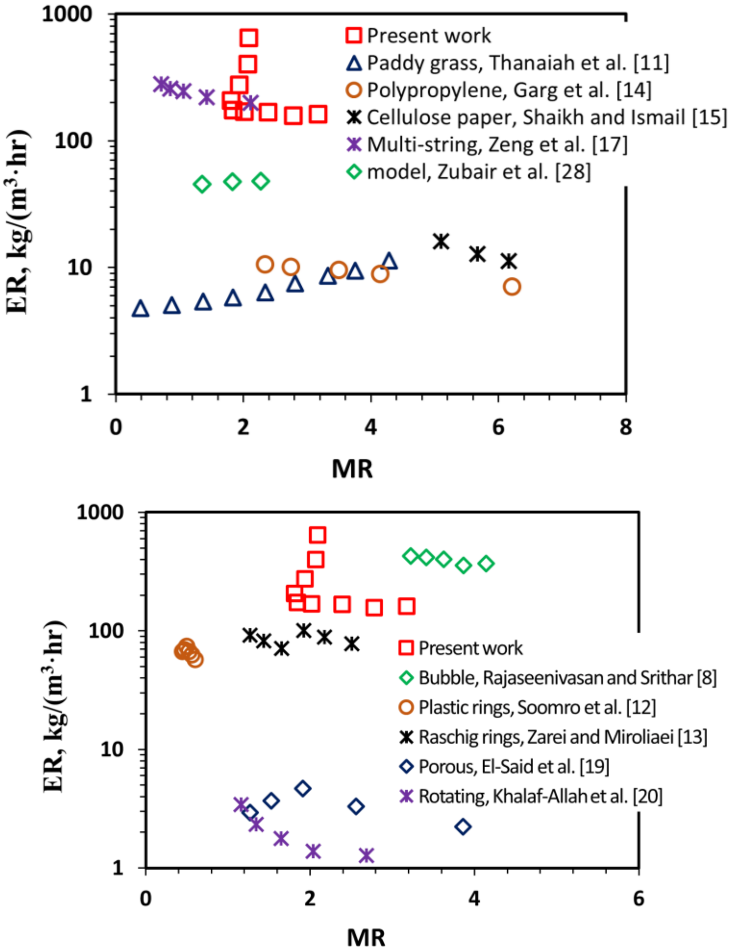

Figure 16. Comparison of the evaporation rate of different types of humidifiers

Figure 17 shows the mean values of η_{hum} for different types of humidifiers. As expected, the bubble column humidifier [8] has the highest value of 0.94. The efficiency of the film humidifier does not reach the maximum values of packing materials (η_{hum}=0.81, [11]) and is positioned between the highest and the lowest performance values of all humidifiers.

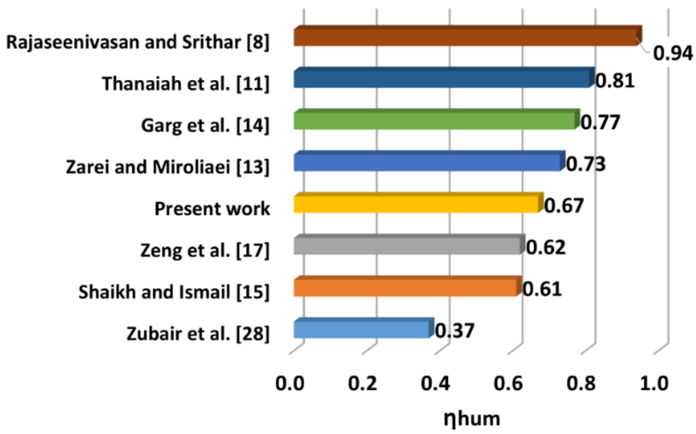

Figure 17. Comparison of thermodynamic performance of different types of humidifiers

Figure 18 shows that a film humidifier has the highest *ER* values at the air pressure drop of approximately 25 Pa/m. The *ER* values of the multi-strand humidifier [17] are 2 times lower, although the pressure losses are significantly lower. A humidifier with hydrophobic plastic packing material [12] has the lowest *ER* values (≈60 kg/m³h) with a pressure drop of approximately 100 Pa/m. The highest pressure drop (7–12 kPa/m) is observed in a bubble column humidifier [8]. At the same time, the *ER* of a bubble column device is 1.5 times lower than that of a film humidifier. Therefore, a film humidifier provides the highest *ER* with one of the lowest air pressure drop.

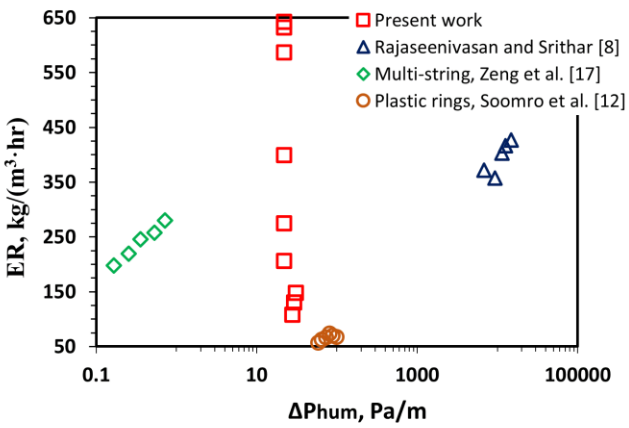

Figure 18. Comparison of air pressure drop of different types of humidifiers

CONCLUSION

A film humidifier in the form of a vertical acrylic tube was experimentally investigated in this study. The advantages of the proposed design include simplicity and a significant surface area of a phase contact per unit volume with a direct and continuous air flow. Low water consumption and the absence of the need for water spraying through nozzles allow for the lowest hydraulic and aerodynamic resistances. From an operational perspective, the most notable operating condition for the film humidifier occurs at $j_a = 0.34$, $MR = 2$ and $t_{w,in} = 60$ °C. These parameters provide the maximum performance ($ER = 642$ kg/m^{3}h) with minimal energy consumption and prevent condensate contamination with water droplets. It requires the following conditions $\varepsilon_{hum} \approx \eta_{hum} \approx 0.6$.

New empirical relations (33) and (34) are suggested for the mathematical model of a film humidifier. These formulae are recommended to be applied for acrylic tubes (with a diameter from 20 to 50 mm and a length from 2 to 3 m) under the following operating conditions of the HDH system: $j_a \leq 0.34$, $MR \leq 2$, and $t_{w,in} \leq 60$ °C. For other conditions, the proposed mathematical model needs to be refined.

A comparison of the energy efficiency indicators of different types of humidifiers showed that the film humidifier demonstrates the highest *ER* across the entire range of *MR* variations. Moreover, the pressure losses for water and air are the lowest, 22.3 kPa and 25 Pa/m, respectively. Thus, using a vertical tube as a humidifier in an HDH system will reduce the desalination unit power and specific energy consumption.

Future research will focus on developing an experimental desalination unit with a fin-tube dehumidifier and conducting studies on optimizing the performance of the humidifier and dehumidifier to improve the overall energy efficiency of small-scale HDH systems.

ACKNOWLEDGMENTS

Yang Liu: Conceptualization, Funding acquisition, Methodology, Writing – review and editing. **Volodymyr Sereda**: Methodology, Investigation, Supervision, Writing – original draft. **Tetiana Podstievaia**: Investigation, Validation, Writing – original draft. **Igor Telychko**: Validation, Visualization, Writing – review and editing.

NOMENCLATURE

Symbols

c_p	specific heat capacity	[J/kgK]
D	diffusion coefficient of water vapour in air	[m²/s]
d	humidifier inner diameter	[m]
E	exergy	[W]
f	friction factor	[–]
F_{hum}	humidifier interphase surface area	[m²]
J	diffusion flux	[kg/m²s]
j	superficial phase velocity	[m/s]
h	specific enthalpy	
h_{con}	convective heat transfer coefficient	[W/m²K]
h_{d}	mass transfer coefficient	[m/s]
h_{vl}	latent heat of water	[J/kg]
m	mass flow rate	[kg/s]
M_a	molar mass of air	[g/mol]
M_{v}	molar mass of water vapour	[g/mol]
N	power	[W]
Nu	Nusselt number	[–]
Pr	Prandtl number	[–]
p_{par}	partial pressure of water vapour in moist air	[Pa]
Q	heat transferred	[W]
R_{a}	specific gas constant of air	[J/kgK]
R_{v}	specific gas constant of water vapour	[J/kgK]
Re_{a}	Reynolds number of moist air	[–]
Re_{f}	film Reynolds number	[–]
s	specific entropy	[J/kgK]
Sc_{a}	Schmidt number of moist air	[–]
Sh	Sherwood number	[–]
t	temperature	[°C]
$t_{\mathrm{a,aver}}$	average temperature of moist air in the humidifier	[K]
V	volume	[m³]
w	velocity	[m/s]
l	length	[m]

Greek letters

Γ	mass flow rate per unit perimeter	[kg/ms]
ΔP	pressure drop	[Pa/m]
ΔT	logarithmic mean temperature difference in the humidifier	[K]
$\Delta\omega$	moisture mass flow rate transferred from water to air	[kg/s]
ε	exergetic efficiency	[–]
η	effectiveness	[–]

λ	thermal conductivity	[W/mK]
μ	dynamic viscosity	[Pa s]
ρ	density	[kg/m³]
ν	kinematic viscosity	[m²/s]
φ	relative humidity of air	[–]
ω	humidity ratio of air	[kg water/kg dry air]

Subscripts and superscripts

a	moist air
calc	calculated
con	convective
evap	evaporation
exp	experimental
hmt	heat and mass transfer
hum	humidifier
id	ideal
in	humidifier inlet
out	humidifier outlet
v	water vapour
w	water

REFERENCES

1. M. Amidpour, M. Salimi, and W. He, Need for low-grade heat-driven desalination systems, *Advances in Sustainable Humidification-Dehumidification Thermal Desalination Systems*, 2025, https://doi.org/10.1016/B978-0-323-95658-1.00001-6.
2. Water, sanitation and hygiene (WASH) | UNICEF. https://www.unicef.org/water-sanitation-and-hygiene-wash [Accessed: May 29, 2026].
3. Subramani A. and Jacangelo J.G., Emerging desalination technologies for water treatment: A critical review, *Water Res.*, Vol. 75, pp 164–187, May 2015, https://doi.org/10.1016/j.watres.2015.02.032.
4. Karhe Y.B. and Walke P.V., A solar desalination system using humidification-dehumidification process - a review of recent research, *International Journal of Modern Engineering Research*, Vol. 3, No. 2, pp 962–969, 2013.
5. A. S. A. Mohamed, M. S. Ahmed, H. M. Maghrabie, and A. G. Shahdy, Desalination process using humidification–dehumidification technique: A detailed review, *International Journal of Energy Research*, Vol. 45, No. 3, pp 3698–3749, 2021, https://doi.org/10.1002/er.6111.
6. Velmurugan V., Prem Kumar S., and Ragul S., Humidificaton-Dehumidification Desalination System - An Overview, *Int. J. Sci. Res. Sci. Technol.*, Vol. 5, No. 4, pp 1163–1177, 2018, www.ijsrst.com, [Accessed: May 30, 2026].
7. Zeller M. and Busweiler U., M8 Humidifying and Drying of Air, in *VDI Heat Atlas*, Springer Berlin Heidelberg, pp 1343–1362, 2010.
8. T. Rajaseenivasan and K. Srithar, An investigation into a laboratory scale bubble column humidification dehumidification desalination system powered by biomass energy, *Energy Convers. Manag.*, Vol. 139, pp 232–244, 2017, https://doi.org/10.1016/j.enconman.2017.02.043.
9. M. Khan, M. Faizan, M. A. Antar, and A. E. Khalifa, Experimental study on optimum performance of two-stage air-heated bubble-column humidification–dehumidification system, *Water SA*, Vol. 49, No. 4, pp 374–386, Oct. 2023, https://doi.org/10.17159/wsa/2023.v49.i4.4009.

10. A. S. Goghari, I. Ghofrani, M. A. Yazdi, E. Golab, and A. Moosavi, Experimental study and economic analysis of a novel humidification-dehumidification system with a two-stage bubble column humidifier and packed bed dehumidifier for high-saline water desalination, *Energy Convers. Manag.*, Vol. 343, Nov. 2025, https://doi.org/10.1016/j.enconman.2025.120255.
11. K. Thanaiah, V. Gumtapure, and G. Mitiku Tadesse, Experimental analysis on humidification-dehumidification desalination system using different packing materials with baffle plates, *Thermal Science and Engineering Progress*, Vol. 22, May 2021, https://doi.org/10.1016/j.tsep.2020.100831.
12. S. Hussain Soomro, R. Santosh, C. U. Bak, C. H. Yoo, W. S. Kim, and Y. D. Kim, Effect of humidifier characteristics on performance of a small-scale humidification-dehumidification desalination system, *Appl. Therm. Eng.*, Vol. 210, Jun. 2022, https://doi.org/10.1016/j.applthermaleng.2022.118400.
13. T. Zarei and M. R. Miroliaei, Performance evaluation of an HDH desalination system using direct contact packed towers: experimental and mathematical modeling study, *Water Reuse*, Vol. 12, No. 1, pp 92–110, Mar. 2022, https://doi.org/10.2166/wrd.2022.095.
14. K. Garg, R. Beniwal, S. K. Das, and H. Tyagi, Experimental investigation of a low-cost humidification-dehumidification desalination cycle using packed-bed humidifier and finned-tube heat exchanger, *Thermal Science and Engineering Progress*, Vol. 41, Jun. 2023, https://doi.org/10.1016/j.tsep.2023.101858.
15. J. S. Shaikh and S. Ismail, Performance evaluation of a solar humidification dehumidification desalination system employing a multistage bubble column dehumidifier, *Solar Energy*, Vol. 263, Oct. 2023, https://doi.org/10.1016/j.solener.2023.111933.
16. A. Mahmoudi, M. S. Valipour, and S. Rashidi, Potentials of porous materials and thermal control system for performance enhancement of humidification-dehumidification desalination unit powered by solar dish collector: Experimental study with 4E analysis, *International Communications in Heat and Mass Transfer*, Vol. 164, 2025, https://doi.org/10.1016/j.icheatmasstransfer.2025.108958.
17. Z. Zeng, A. Sadeghpour, and Y. S. Ju, A highly effective multi-string humidifier with a low gas stream pressure drop for desalination, *Desalination*, Vol. 449, pp 92–100, Jan. 2019, https://doi.org/10.1016/j.desal.2018.10.017.
18. E. M. S. El-Said, M. A. Dahab, M. Omara, and G. B. Abdelaziz, Solar desalination unit coupled with a novel humidifier, *Renew. Energy*, Vol. 180, pp 297–312, 2021, https://doi.org/10.1016/j.renene.2021.08.105.
19. E. M. S. El-Said, M. A. Dahab, M. A. Omara, and G. B. Abdelaziz, Humidification-dehumidification solar desalination system using porous activated carbon tubes as a humidifier, *Renew. Energy*, Vol. 187, pp 657–670, 2022, https://doi.org/10.1016/j.renene.2022.01.023.
20. R. A. Khalaf-Allah, G. B. Abdelaziz, M. G. Kandel, and A. S. Easa, Development of a centrifugal sprayer-based solar HDH desalination unit with a variety of sprinkler rotational speeds and droplet slot distributions, *Renew. Energy*, Vol. 190, pp 1041–1054, May 2022, https://doi.org/10.1016/j.renene.2022.04.019.
21. Welcome to CoolProp — CoolProp 7.2.0 documentation. https://coolprop.org/ [Accessed: May 30, 2026].
22. V. Voloshchuk, P. Gullo, E. Nikiforovich, and N. Buyak, Simulation and Exergy Analysis of a Refrigeration System Using an Open-Source Web-Based Interactive Tool—Comparison of the Conventional Approach and a Novel One for Avoidable Exergy Destruction Estimation, *Applied Sciences,* Vol. 11, No. 23, 11535, Dec. 2021, https://doi.org/10.3390/app112311535.
23. F. Nematollahi, A. Rahimi, and T. T. Gheinani, Experimental and theoretical energy and exergy analysis for a solar desalination system, *Desalination*, Vol. 317, pp 23–31, 2013, https://doi.org/10.1016/j.desal.2013.02.021.

24. Holman J. P., *Experimental methods for engineers*. 8th ed., McGraw-Hill, New York, 2012.
25. P. Barabash, A. Solomakha, V. Sereda, N. Prytula, P. Strynada, and Y. Liu, Heat and mass transfer of countercurrent air-water flow in a vertical tube, *Heat and Mass Transfer,* Vol. 59, No. 7, 2023, https://doi.org/10.1007/S00231-023-03342-2.
26. K. W. McQuillan and P. B. Whalley, A comparison between flooding correlations and experimental flooding data for gas-liquid flow in vertical circular tubes, *Chem. Eng. Sci.*, Vol. 40, No. 8, pp 1425–1439, Jan. 1985, https://doi.org/10.1016/0009-2509(85)80083-X.
27. H. Schmidt, A. Wellenhofer, S. Muschelknautz, J. Schmidt, F. Schmidt, D. Mewes, A. Mersmann, and J. Stichlmair, L2 Two-Phase Gas-Liquid Flow, *VDI Heat Atlas*, pp 1117–1180, 2010, https://doi.org/10.1007/978-3-540-77877-6_78.
28. M. I. Zubair, F. A. Al-Sulaiman, M. A. Antar, S. A. Al-Dini, and N. I. Ibrahim, Performance and cost assessment of solar driven humidification dehumidification desalination system, *Energy Convers. Manag.*, Vol. 132, pp 28–39, Jan. 2017, https://doi.org/10.1016/j.enconman.2016.10.005.
29. W. Zhong, T. He, and J. Longtin, Pulsed laminar falling films in vertical tubes: Maintaining a continuous liquid film with reduced film thickness, *Exp. Therm. Fluid Sci.*, Vol. 113, 2020, https://doi.org/10.1016/j.expthermflusci.2019.110011.
30. M. H. Sharqawy, M. A. Antar, S. M. Zubair, and A. M. Elbashir, Optimum thermal design of humidification dehumidification desalination systems, *Desalination*, Vol. 349, pp 10–21, 2014, https://doi.org/10.1016/j.desal.2014.06.016.
31. P. Barabash, A. Solomakha, and V. Sereda, Experimental investigation of heat and mass transfer characteristics in direct contact exchanger, *Int. J. Heat Mass Transf.*, Vol. 162, 120359, 2020, https://doi.org/10.1016/j.ijheatmasstransfer.2020.120359.

Paper submitted: 17.02.2026
Paper revised: 04.06.2026
Paper accepted: 12.06.2026